Archaeometry **51**, 5 (2009) 808–821 doi: 10.1111/j.1475-4754.2008.00451.x

USING OPTICAL COHERENCE TOMOGRAPHY TO EXAMINE THE SUBSURFACE MORPHOLOGY OF CHINESE GLAZES

M.-L. YANG[1]†, AMY M. WINKLER[2], JENNIFER K. BARTON[3] and PAMELA B. VANDIVER[1]

[1]*The Heritage Conservation Science Program in the Department of Materials Science and Engineering, University of Arizona, Tucson, AZ 85721-0012*
[2]*The College of Optical Sciences, University of Arizona, Tucson, AZ 85721-0094*
[3]*Division of Biomedical Engineering, University of Arizona, Tucson, AZ 85721-0240*

Optical coherence tomography (OCT), a new method for ceramics research, is a non-destructive, three-dimensional tomography system, which provides subsurface morphology visualization of samples based on the refractive index or dielectric constant differences in the target specimen. In this study, seven shards from different Chinese kilns of Song and Yuan dynasties (10–14th centuries) were scanned to visualize the subsurface morphology of their glazes. The images revealed unique phase assemblage modes in different samples. The results suggest that OCT may be used to identify ceramics and provide information about their manufacturing technology.

KEYWORDS: OPTICAL COHERENCE TOMOGRAPHY, GLAZE, SUBSURFACE MORPHOLOGY, CERAMIC, CHINA

INTRODUCTION

Chinese glazes display various aesthetic characteristics, based on the assemblage of the three basic phase states: (1) a homogeneous glassy phase; (2) a liquid–liquid phase separated state; and (3) a crystallized phase structure. The three types of phase can exist alone, or two or all three types may co-exist in a glaze, depending on the composition, thermal history and cooling rate used in the manufacturing processes. According to a contemporary Song Dynasty (10–14th centuries) literati's record, Ding ware was too shiny to be admitted into the palace (Lu 1996). Therefore, a kind of less shiny glaze was regarded as being the highest aesthetic for Chinese ceramics. Thus, producing a less shiny glaze was the most important challenge for Song dynasty pottery workshops. With compositions regulated, firing temperature and atmosphere controlled, cooling rates modified, additive experimental testing and other parameters measured, ceramic manufacturing technologies flourished during the Song Dynasty.

Many analytical methods to identify the phase structure of Chinese glazes have been used in the past three decades, such as scanning electron microscopy (SEM) and transmission electron microscopy (TEM) (Kingery and Vandiver 1983; Vandiver and Kingery 1984; Li *et al.* 2001, 2005; Zhang *et al.* 2002). However, most sampling methods are destructive. They are not suitable for most museum collections or intact objects. In addition, the analysis of variability is limited by the small sampling size. Therefore, the variability of workshop production may not be reflected in the analytical result.

Received 30 May 2008; accepted 22 September 2008
†Corresponding author: meiliy1@email.arizona.edu

However, optical coherence tomography (OCT) provides a non-destructive, three-dimensional technique and is a new method for conducting ceramics research. It displays the cross-sectional subsurface morphology of samples based on the varied refractive index or dielectric constant. Therefore, the variation of brightness in the image, typically a grey scale variation from black to white, actually relates to the variation in local components and phase assemblage. White pixels typically correspond to regions of high reflectivity or backscatter in the sample, whereas the black pixels correspond to weak backscattering conditions (Fujimoto 2002).

In the present paper, we selected seven shards for two-dimensional imaging of their subsurface morphologies. Referring to previous research on these Chinese glaze samples from known kilns, we classify these samples into four categories that not only exhibit various characteristics of glaze, but also reveal various manufacturing technologies used in the kiln firing. The results provide not only a macroscopic view of the glaze structure, but also a convenient method for interpreting the ceramic technology and perhaps may aid in identifying the special practices of some kilns. Furthermore, they may provide the ceramic or glass conservator with additional information about the weathering, crazing and bubble structure of certain ceramics. One of the authors has confirmed this technique useful in the authentication of jade (Yang *et al.* 2004), and current studies include an assessment of authenticity.

THE OCT METHOD

Optical coherence tomography (OCT) utilizes time-gated, backscattered light to create cross-sectional images in a material. This technique is similar to ultrasound, which times an ultrasound pulse returned from impedance mismatches in a sample. Similarly, OCT signals come from index of refraction mismatches.

A system diagram is shown in Figure 1. The light source is a superluminescent diode (Superlum Broadlighter, Moscow, Russia) with 890 nm centre wavelength and 150 nm

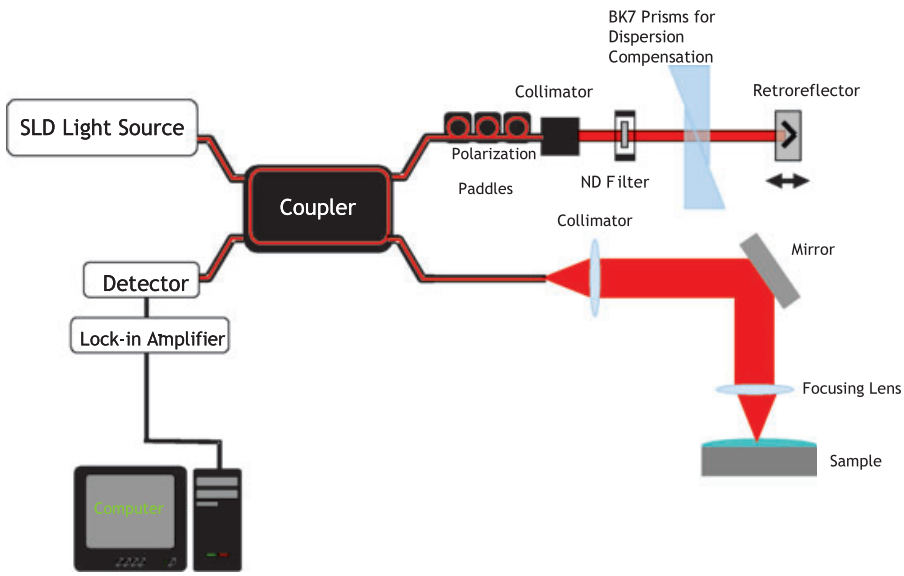

Figure 1 *OCT system schematic.*

bandwidth, resulting in a theoretical coherence length of approximately 2.3 μm in air or 1.5 μm in a silicate glaze (assuming a refractive index of 1.5). The light is split by a 50:50 Corning HI780 fibre coupler (AC Photonics, Santa Clara, CA, USA). The sample arm consists of collimating and focusing lenses. The numerical aperture (NA) of the focusing lens is approximately 0.1, providing a measured lateral resolution of approximately 10 μm. The reference arm consists of a collimating lens and retroreflector, oscillating at 14 Hz. Glass prisms (BK7) are introduced in the reference arm to match glass dispersion in the sample arm. This dispersion compensated axial point spread function is approximately 4.5 μm in air or 3.0 μm in glaze, and we thus assume a depth resolution of 3.0 μm in the glazes.

In the images, the spatial resolution is limited by the optical system, which is 10 μm laterally and 3.0 μm axially. Since most glazes are transparent or translucent in the near infrared, they allow penetration to a considerable depth. Backscattering in our glaze samples limited the depth of imaging to 0.4–0.5 mm. However, sometimes it is deeper, depending on the medium environment. For example, in the homogeneous glassy phase, the depth is probably over 1 mm.

INTRODUCTION OF SAMPLES

We have used OCT to study seven samples of Chinese glazed ceramics that have been characterized previously. Microanalysis of compositions was conducted for the samples using elemental probe micro-analysis (EPMA) and microstructures were characterized by SEM and TEM with simultaneous energy dispersive X-ray analysis (Kingery and Vandiver 1983; Kingery *et al.* 1983; Tite *et al.* 1984; Vandiver and Kingery 1984, 1985). Some visible descriptive information about these samples is listed in Table 1. For all samples, the inevitable bubbles vary in size; whereas crazing is uncommon. The shards were sampled from shard study collections of various museums.

To characterize bubbles imaged with OCT, an air bubble standard was created in a piece of glass. The air bubble within this glass was characterized by two parallel, bright, short lines indicating high reflectivity at the air–glass interface, allowing us to distinguish between bubbles and the homogeneous glassy phase in the OCT image (Fig. 2). The upper and lower bright, short lines indicate the top and bottom of this bubble. However, around the sides of the bubble, light is reflected out of detection range, resulting in a lack of a consistent outline of the bubble in OCT. Therefore, the typical image of a bubble in a homogeneous glass, called ‘glass bubble’, is two parallel, bright, short lines or dots in our OCT images.

ANALYSIS AND RESULTS

If we ignore the bubbles, this research allows us to group our samples into four categories of phase assemblages: mode one is only a homogeneous glassy phase; mode two is a homogeneous glassy phase and crystallized phases; mode three is the liquid–liquid phase separation and crystallized phases with very little or no single glassy phase; and mode four is the homogeneous glassy phase and liquid–liquid phase-separated phase and crystallized phase. All samples exhibit varying amounts and sizes of bubbles. Crazing occurs only in certain samples (see Table 1).

Mode one is a homogeneous glassy phase with some bubbles. As shown by the Qingbai 15885 sample, for the glaze section, the OCT image displays a dark area indicating almost no backscatter except for some bubbles indicated by collinear pairs of bright dots or short lines (Fig. 3). The bubbles are distributed near the interface area of the glaze–body,

Table 1 *Information on samples, O: present; X: not present*

Sample name	*Thickness (mm) of glaze/ body*	*Colour of glaze/ body*	*Bubble*	*Crazing*	*Date and origin of sample*
Ru #2	Around 0.5/ Less than 3	Blue-green/ grey	O	O	10–12th c/ coll. of Shanghai Institute of Ceramics Museum
Ru #4	Less than 0.5/ Around 3	Grey-green/ white	O	O	10–12th c/ coll. of Shanghai Institute of Ceramics Museum
Jun 1909.4-1.26 (BM)*	Around 3/ 4.5	Milky Blue/ Grey-black	O	X	13–14th c/ coll. of the British Museum from Yuxian, Henan
Guan #1	Less than 1/ Around 3 or thicker	Blue-green/ dark red-brown	O	O	12–13th c/ coll. of the University of Michigan Museum of Art from Hangzhou, Zhejiang
Longquan L-2a†	Around 1/ Around 3	Grey-green/ Grey-white	O	X	12–13th c/ coll. of Museum of Far Eastern Antiquities Stockholm, Sweden. Palmgren collected from Dayao, Longquan, Zhejiang
Qing-bai 15885 (BM)‡	Less than 0.2/ Around 2	Light Blue-white/ white	O	X	13–14th c/ coll. of the British Museum from Jingdezhen, Jiangxi
Jianyang #5	Around 0.2/ Around 5	Black with foxy-red specks/ dark red brown	O	X	12–13th c/ coll. of the University of Michigan. Cox collected from Jianyang, Fujian

*The sample is no. 19 in Vandiver and Kingery, 1985.
†The sample number is same as Vandiver and Kingery, 1984.
‡The sample is no. 35 in Vandiver and Kingery, 1985.

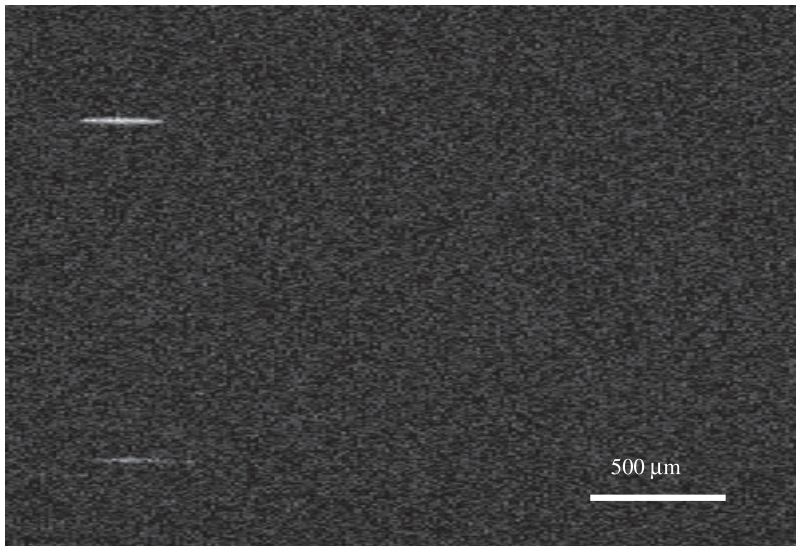

Figure 2 *OCT revealed the 'glass bubble' image, an air bubble within the glass. The bubble is characterized by two parallel, bright, short lines indicating high reflectivity at the air–glass interface. However, around the sides of the bubble, light is reflected out of detection range.*

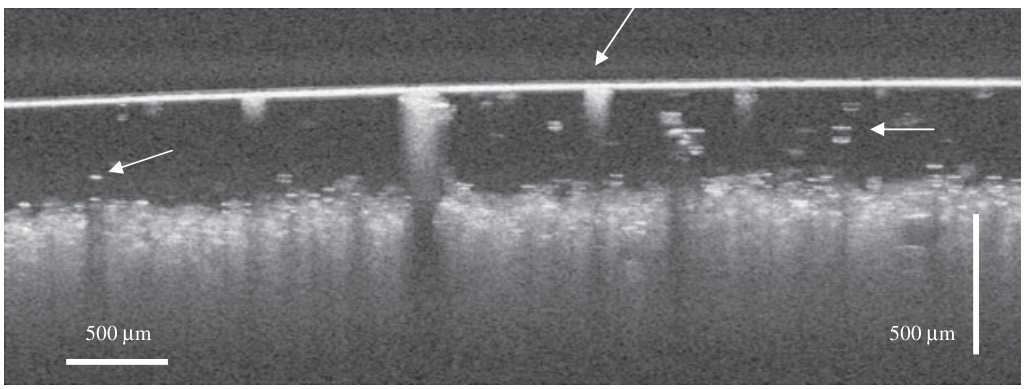

Figure 3 *The glaze on the Qing-bai 15885 sample is free of the light-scattering homogeneous glassy phase with bubbles, indicated by two, parallel, bright, short lines or dots (left and right arrows). However, the cone-shaped, bright nodules indicate iron oxide impurities in the glaze (central arrow).*

indicating outgassing of the body and rapid firing of the glaze to the point at which the glaze surface fuses.

The sample also exhibits many amber spots on the surface, varying in size. However, according to previous analysis, the iron concentration near the surface area is higher than the mean areas of the glaze (Vandiver and Kingery 1985). In the image, those amber spots, indicating iron oxide impurities, are represented as bright, cone-shaped nodules.

Similar to the Qing-bai sample, the Jianyang #5 sample consists of a homogeneous glassy phase with few bubbles and considerably abundant iron oxide precipitate within the glaze

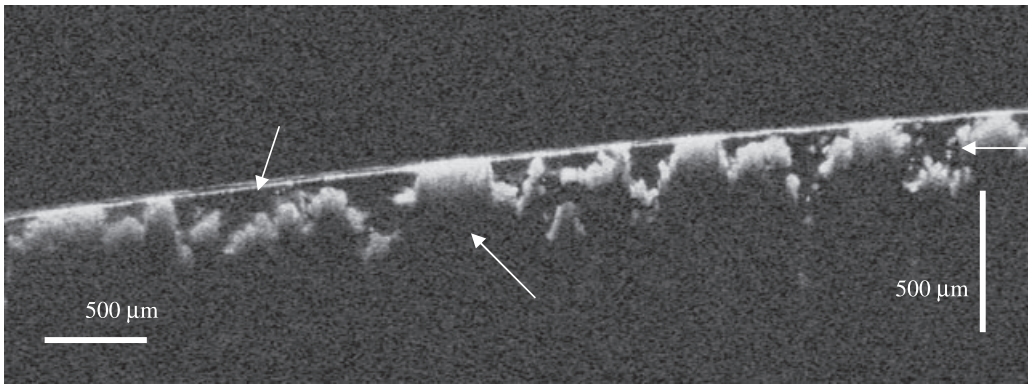

Figure 4 *The glaze on the Jianyang #5 sample exemplifies the homogeneous glassy phase with only a few bubbles (right arrow) and considerably abundant iron oxide precipitation concentrated on the surface area of the glaze. The left arrow points to a glassy phase section, whereas the central arrow points to a section without signal, under the white section, due to no light source penetrating the opaque iron oxide precipitates.*

(Fig. 4). A large amount of specks in the dark glaze are visible with the naked eye, and radiating, compact, platy, grey-black crystal masses are observed with the microscope. These probably consist of abundant iron oxide precipitates, hematite (Fe_2O_3, $n_\omega = 3.22$, $n_\varepsilon = 2.94$). A ferric oxide in Jian ware is usually formed during the cooling process in a fully oxidizing atmosphere (Wood 1999). The OCT image exhibits iron oxide precipitation, an opaque mineral, concentrated near the surface area of glaze. These noteworthy characteristics, the scarceness of bubbles and the surface-concentrated iron oxide precipitation in the Jianyang glaze sample probably suggest that a slower firing rate was employed, and a fully oxidizing atmosphere was provided during the cooling process.

Mode two, shown in Figure 5 (a) and 5 (b), is a homogeneous glassy phase with one or more crystallized phases. The Longquan L-2a sample has been analysed previously by SEM, and was found to have no liquid–liquid phase separation, whereas some crystals, such as anorthite and wollastonite, and a few undissolved crystals, such as quartz, are formed in the cooling process (Vandiver and Kingery 1984). The OCT image reveals the morphology of the subsurface to include not only a simple homogeneous glassy phase with lots of bubbles, indicated by the parallel, collinear, bright pairs of dots, but also some crystal structures, indicated by discrete nodules of grey-scale variation. For example, anorthite crystal structure is in grey nodules, whereas wollastonite is in brighter nodules (Fig. 5 (a)). The distribution of bubbles is quite even in the glaze (Fig. 5 (b)). It also implies that the firing rate of the Longquan sample is slower than that of the Qing-bai in our case.

Distinguishing anorthite, wollastonite and quartz crystals depends primarily on differences in refractive index (n) compared to the glassy phase and to each other. The greater the refractive index, the greater the brilliance (gloss) will be in the glaze (Shaw 1971). Therefore, according to the differences of refractive indices between the three crystalline components and the homogeneous glass ($n = 1.5$), the index of wollastonite ($n_\alpha = 1.616–1.640$, $n_\beta = 1.628–1.650$, $n_\gamma = 1.631–1.653$) has the largest difference, followed by anorthite ($n_\alpha = 1.577$, $n_\beta = 1.585$, $n_\gamma = 1.590$), and finally quartz ($n_\omega = 1.544$, $n_\varepsilon = 1.553$). Both wollastonite and anorthite are biaxial materials with birefringence (Ehlers 1987). Based on our estimations, it is apparent that the wollastonite is represented by more brilliant white in the image due to its strong scattering. By contrast, the grey section with somewhat clustered nodules represents anorthite crystals.

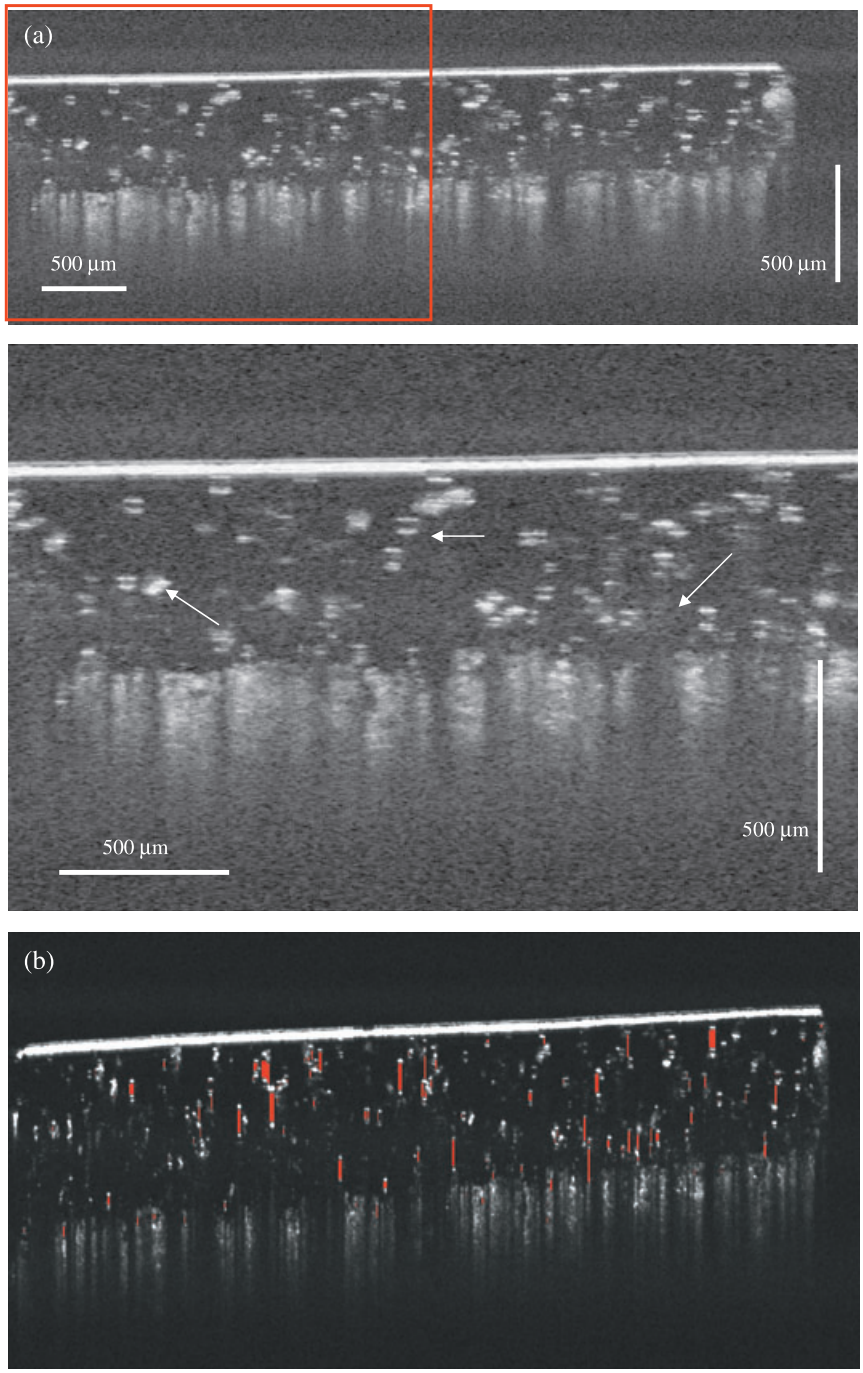

Figure 5 *(a) The glaze on the Longquan L-2a sample exemplifies the homogeneous glassy phase, a small amount of crystallized anorthite (grey nodules, right arrow), wollastonite (white nodules, left arrow) and more 'glass bubbles' (the central arrow points to two bubbles). (b) The bubbles are almost marked off in short red lines. The bubbles are evenly distributed in the glaze of the Longquan L-2a sample. The image is the same as (a) using a different scale.*

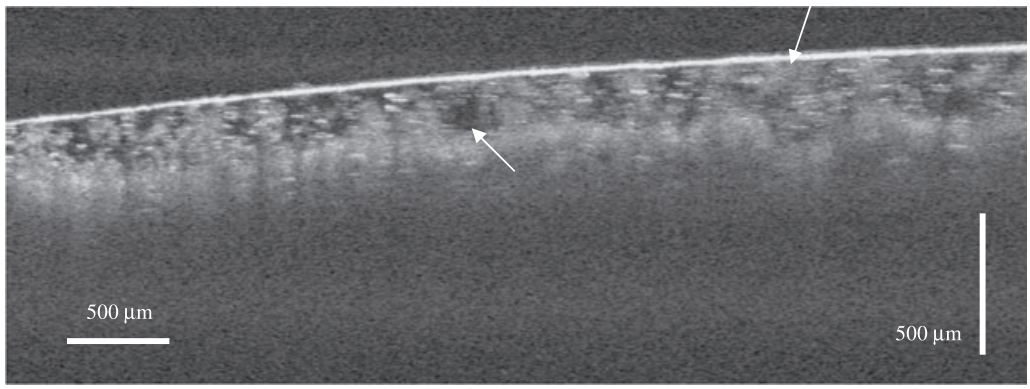

Figure 6 *The glaze on the Guan #1 sample illustrates the homogeneous glassy phase (dark section, left arrow) and crystallized phases with bubbles. Anorthite (grey section, right arrow) is abundant in the clusters. However, because the abundant anorthite layer is between the glaze and body, sometimes it is not easy to distinguish one from the other.*

The other example of mode two is the Guan #1 sample. However, it displays differences from the Longquan L-2a sample. In general, Guan glaze has sufficient anorthite crystallization within its homogeneous glassy phase glaze and sometimes partially undissolved constituents (Vandiver and Kingery 1985; Li *et al.* 2001). The image exhibits abundant grey clusters, which are anorthite crystals, sometimes extending from the interface of glaze–body into glaze, occupying a considerable portion of the glaze (Fig. 6). The presence of an anorthite layer between glaze and body probably implies a high temperature with longer firing time and some heterogeneous nucleation at the interface between glaze and body in the manufacture process of the Guan sample.

Mode three consists of liquid–liquid phase separation with crystallized phases. The typical representative of the time period is the Jun 1909.4-1.26 sample (Fig. 7). The sample has an

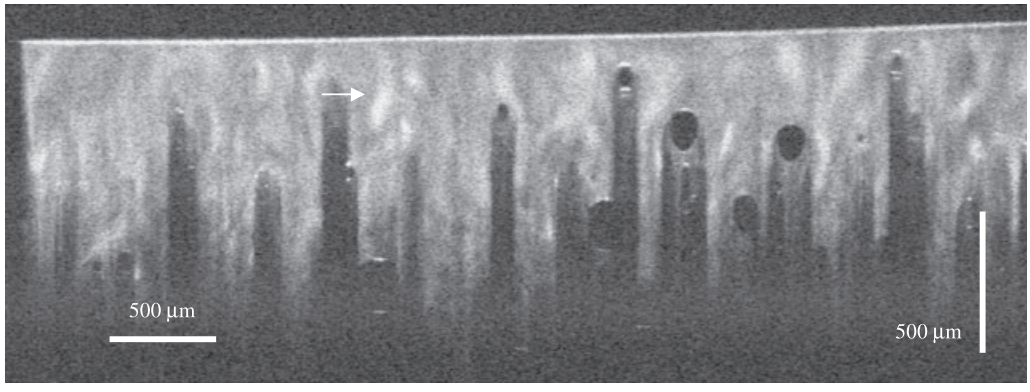

Figure 7 *The glaze on the Jun 1909.4-1.26 sample illustrates the liquid–liquid phase separation phase and pseudowollastonite crystallized phase. The white streaks are pseudowollastonite structures (arrow); whereas the grey background with white streaks is the liquid–liquid phase separation. The black ellipse with top and bottom brilliant dots is the 'l-l phase separation bubble.'*

almost opaque milky blue glaze under natural light. Except for some bubbles, the whole image can be divided into a somewhat even grey background and streaky white sections. The white streaks indicate pseudowollastonite-rich structures and the almost uniform grey background is the liquid–liquid phase separated structure. Both are entangled or intermingled with each other. According to previous research, a finer milling and better mixing of raw materials probably operated in the manufacturing process, which caused visual uniformity in the texture of the glaze (Vandiver and Kingery 1985). The bubble with top and bottom brilliant dots possesses a distinct outline, called a 'l-l phase separation bubble', which is different from a 'glass bubble' without outline.

Phase separation in glass or glaze has been an important research issue since the 1960s (Shaw and Uhlmann 1969; Li and Uhlmann 1970; Uhlmann and Kolbeck 1976; Simmons 1977; Mazurin and Porai-Koshits 1984). It is a complicated process of undercooling two compositions that are more stable when unmixed, similar to an emulsion of oil and water. A complex thermal history involves maintaining a sufficient undercooled temperature of sometimes as little as 20°C and low enough viscosity for sufficient time to permit the emulsion formation. However, liquid–liquid phase separation causes a structural rearrangement of the homogeneous glass that changes the density and refractive index of the original glassy phase (Simmons 1977).

A borosilicate glass, here treated to promote liquid–liquid phase separation with the refractive index $n = 1.52$, was imaged with OCT. The image displays uniform structure in a grey scale with a typical 'l-l phase separation bubble', indicated by the top and bottom brilliant dots within a distinct elliptical outline (Figs 8 (a) and 8 (b)). This structure is noticeably different from that of the crystallized phases, allowing the two phases to be distinguished from one another in the Jun 1909.4-1.26 sample. In fact, these characteristics, the uniform structure and bubble outline, are powerful aids for identifying liquid–liquid phase-separated phase in the Jun 1909.4-1.26, Ru #2 and Ru #4 samples.

Mode four is the homogeneous glassy phase, liquid–liquid phase separation and crystallized phase assemblages. The image displays the subsurface morphology of the Ru #2 sample (Fig. 9 (a)). Compared to the SEM image of the sample (Fig. 9 (b)), the complicated structure of anorthite, pseudowollastonite, liquid–liquid phase separation and glass phases can be distinguished. The discrete dark portion, except for some bubbles, is free of light-scattering, indicating homogeneous glass. In contrast, the rest of the section is occupied by a delicate structure of anorthite and pseudowollastonite clusters surrounded by liquid–liquid phase-separated phase. Anorthite appears to take up the majority of the grey volumes with pseudowollastonite appearing scattered throughout, as indicated by smaller, brighter nodules in the glaze. However, compared with the Guan or Jun samples, the phase structure of the Ru #2 glaze is constructed in a more compact, finer-scale arrangement.

According to previous research, in general, the liquid–liquid phase separation volume in the Ru ware is lower than in the Jun ware (Zhang *et al.* 2002). Even so, referring to 'l-l phase separation bubble' locations, the liquid–liquid phase-separated phase can be identified in the Ru #2 sample.

The glaze of the Ru #4 sample visually appears somewhat shinier than the Ru #2. The OCT image reveals a considerable volume of liquid–liquid phase separation in the glaze (Fig. 10 (a)). Two very distinct 'l-l phase separation bubbles' are present, indicating the somewhat abundant liquid–liquid phase separation in the glaze. In contrast, the anorthite is less, and the structure is looser than the Ru #2. A SEM image of the Ru #4 sample is provided, indicating the abundant liquid–liquid phase separation with some pseudowollasotnite crystals (Fig. 10 (b)). The comparison between the Ru #2 and the Ru #4 samples also provides a criterion to

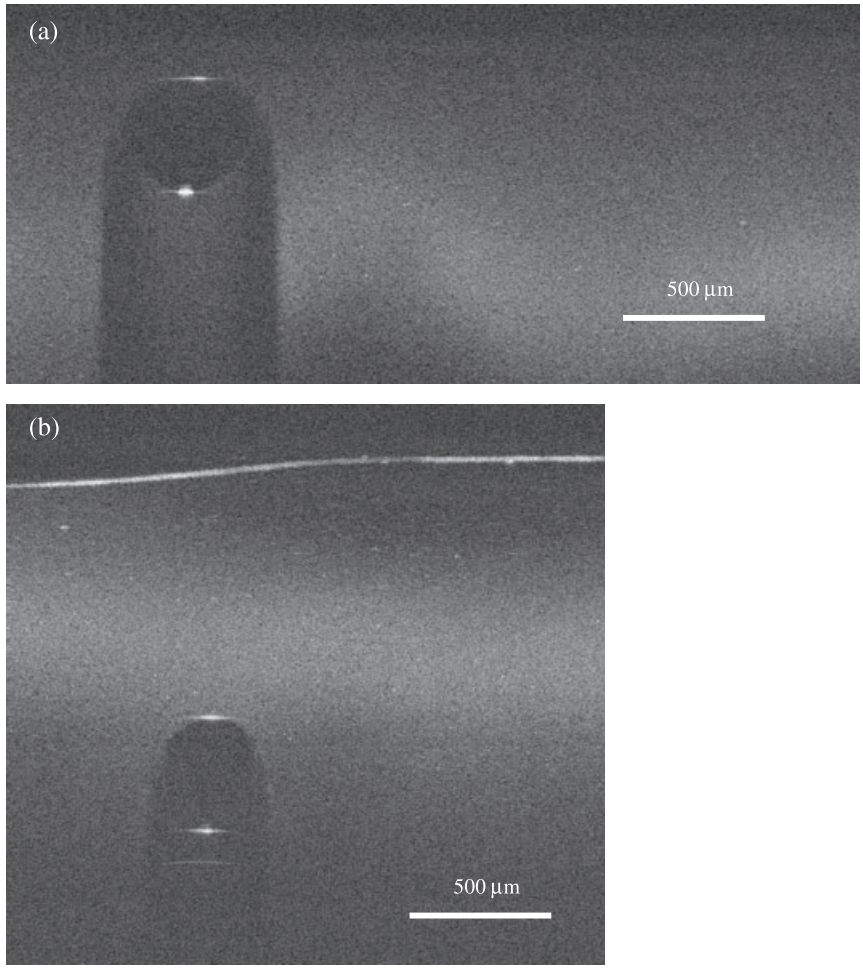

Figure 8 *The two images present a bubble within a borosilicate liquid–liquid phase separated glass with light focused at different depth. Basically, the liquid–liquid phase separation background is uniform. Grey-scale variation is an artefact, due to the fixed focus of the light beam in the sample. The typical 'l-l phase separation bubble' with the shadowing effect is also present below the bubble.*

differentiate the quality of Ru ware. In general, the Ru #2 is evaluated to be of better quality than the Ru #4 by ceramics collectors.

DISCUSSION AND CONCLUSION

Four different phase assemblages were demonstrated by imaging our samples. Every mode displays unique structural components, visualized as various grey scale textures, which are dependent on refractive index, particle size and density of particles. However, according to the variability in texture of the images, the OCT images provide significant information on Chinese ceramics that was acquired using non-destructive methods.

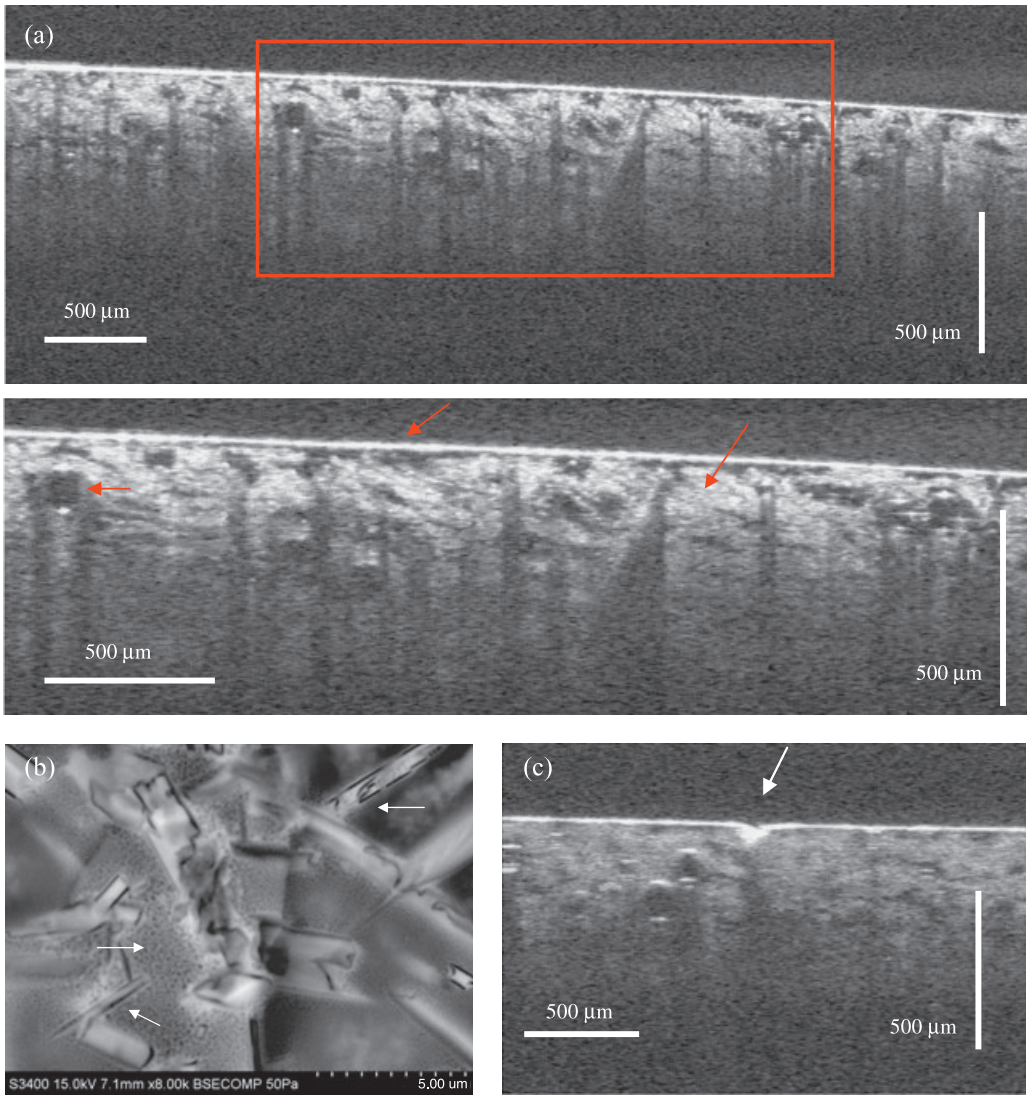

Figure 9 *(a) The glaze on the Ru #2 sample illustrates the homogeneous glassy phase with liquid–liquid phase separation and crystallized phase. Some non-bubble dark portions are homogeneous glassy phase (central arrow), especially close to the surface. There are a few 'l-l phase separation bubbles' (left arrow) in the glaze. The distinct, structural grey section is anorthite crystals (right arrow). However, a few brighter nodules in grey section are pseudowollastonite. (b) The SEM image of the Ru #2 sample reveals the structure of anorthite, liquid–liquid phase separation and glass phase. The needle or column shapes are anorthite crystals (lower arrow), surrounded by liquid–liquid phase separation phase (central arrow) and glass phase (upper arrow). The sample was etched in 1% HF for 10 s. (c) A crack (arrow) in the Ru #2 sample is displayed in the image.*

For the fields of art history and technological history, the results provide powerful criteria for identifying artifactual variability as well as evidence for interpreting aesthetics and technologies of ceramic manufacture. For example, according to the contemporary literati's record, the potters of the Guan kilns were ordered to manufacture ceramics similar to Ru ware

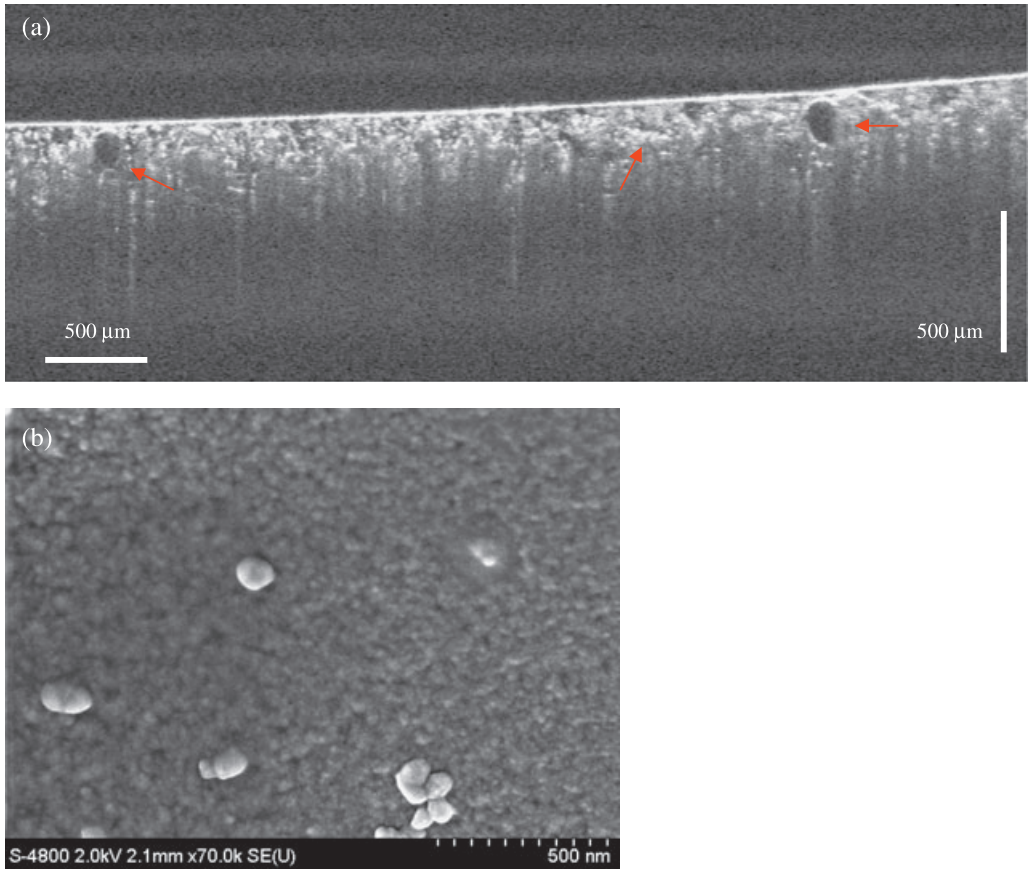

Figure 10 *(a) The glaze on the Ru #4 sample reveals that the less structural grey background occupies much more area, indicating that the liquid–liquid phase separation is abundant, with distinct 'l-l phase separation bubbles' (right and left arrows). In addition, there are more pseudowollastonite precipitates (central arrow) than in the Ru #2 sample. (b) The SEM image of the Ru #4 sample reveals the spherical precipitates of pseudowollastonite formed in liquid–liquid phase separation environments. The sample was etched in 1% HF for 10 seconds.*

quality porcelain. Unfortunately, they were not completely successful. In fact, in the OCT images, Guan and Ru have considerably different phase assemblages. The unique manufacturing technology of Ru ware is not easy to imitate, either by contemporary or later potters.

The results also provide information that is useful in evaluating porcelain in museum collections. The characteristics of a collection can be determined quickly—less than one second for an image measuring 1 mm × 1 mm—and they enable detection of impurities and glaze flaws, such as iron oxide impurities in the Qing-bai and Jianyang samples, or cracks in the Ru sample (Fig. 9b). This information is important for ceramics preservation (McCracken 1992; Vandiver 1992).

In fact, OCT is an ideal materials analysis technique. It has been widely used for examining some museum collections, especially transparent and translucent materials, such as jade (Yang *et al.* 2004), ceramic glazes (Targowski *et al.* 2004), enamels and glass. In addition, it is also

suitable for examining painting (Liang *et al.* 2004, 2005; Adler *et al.* 2007; Latour *et al.* 2007; Targowski 2008; Targowski *et al.* 2008).

However, many components in glazes are birefringent, such as the anorthite, wollastonite and quartz. These components possess polarization properties that can be detected with polarization-sensitive optical coherence tomography (PS-OCT) (de Boer *et al.* 1999; Wiesauer *et al.* 2007). PS-OCT is likely to be a useful technique that we hope to utilize to further characterize these materials.

Furthermore, the texture analysis technique has also been employed previously with OCT images of biological tissue to differentiate tissue types with high correct classification rates (Gossage *et al.* 2003). Arguably, the textural differences between glaze constituents in OCT images is much greater than between these biological tissues, suggesting that texture analysis could also be employed successfully in detailed ceramics analysis.

A future implementation could include a hand-held probe, such as those already in use for OCT imaging of the eye, which can be brought directly to the surface of an item of interest for quick evaluation. Moreover, by multiple scans and image processing, OCT can extend the information derived from a two-dimensional image into a three-dimensional image. Even though some other techniques can produce non-destructive, three-dimensional images of ceramics, such as the X-ray microtomography technique (Dunsmuir *et al.* 1995), OCT possesses some advantages, such as more flexibility with sample size and faster imaging.

ACKNOWLEDGEMENTS

We greatly appreciate use of shards from many museum study collections, and in particular wish to thank Bo Gyllensvard, Jessica Rawson, Li Jiazhi and Lambertus van Zelst. We also thank Joseph Simmons for use of one of the phase separated glasses made in his laboratory, and the Achievement Rewards for College Scientists (ARCS) for providing funding for this study.

REFERENCES

Adler, D. C., Stenger, J., Gorczynska, I., Lie, H., Hensick, T., Spronk, R., Wolohojian, S., Khandekar, N., Jiang, James Y., Barry, S., Cable, Alex E., Huber, R., and Fujimoto, J. G., 2007, Comparison of three-dimensional optical coherence tomography and high resolution photography for art conservation studies, *Optics Express*, **15**, 15972–86.

de Boer, J. F., Milner, T. E., and Nelson, J. S., 1999, Determination of the depth-resolved Stokes parameters of light backscattered from turbid media by use of polarization-sensitive optical coherence tomography, *Optics Letters*, **24**, 300–2.

Dunsmuir, J. H., Vandiver, P. B., Chianelli, R. R., Deckman, H. W., and Hardenbergh, J. H., 1995, X-ray micro-tomography of ceramic artifacts, *Materials Research Society Symposium Proceedings*, **352**, 73–83.

Ehlers, E. G., 1987, *Optical mineralogy: mineral descriptions*, Blackwell Scientific Publications, Palo Alto.

Fujimoto, J. G., 2002, Optical coherence tomography introduction, in Bouma, B. E. and Tearney, G. J. (eds), *Handbook of optical coherence tomography*, 1–40, Marcel Dekker, Inc., New York.

Gossage, K. W., Tkaczyk, T. S., Rodriguez, J. J., and Barton, J. K., 2003, Texture analysis of optical coherence tomography images: feasibility for tissue classification, *Journal of Biomedical Optics*, **8**, 570–5.

Kingery, W. D., and Vandiver, P. B., 1983, Song dynasty Jun (Chun) ware glazes, *The American Ceramic Society Bulletin*, **62**, 1269–74.

Kingery, W. D., Vandiver, P. B., Huang, I.-W., and Chiang Y.-M., 1983, Liquid-liquid immiscibility and phase separation in the quaternary systems K_2O-Al_2O_3-CaO-SiO_2 and Na_2O-Al_2O_3-CaO-SiO_2. *Journal of Non-Crystalline Solids*, **54**, 163–71.

Latour, G., Moreau, J., Elias, M., and Frigerio, J.-M., 2007, Optical coherence tomography: non-destructive imaging and spectral information of pigments, *Proceedings of SPIE*, **6618**, 661806-1–661806-9.

Li, J. H., and Uhlmann, D. R., 1970, The flow of glass at high stress levels: II. The effect of phase separation on viscosity, *Journal of Non-Crystalline Solids*, **3**, 205–24.

Li, J.-Z., Deng, Z.-Q., and Xu, J.-M., 2001, Technical studies and replication of Guan ware: an ancient Chinese ceramic, *MRS Bulletin*, **26**, 31–7.

Li, W.-D., Li, J.-Z., Deng, Z.-Q., Wu, J., and Guo, J.-K., 2005, Study on Ru ware glaze of the northern Song dynasty: one of the earliest crystalline-phase separated glazes in ancient China, *Ceramics International*, **31**, 487–94.

Liang, H.-D., Cid, M. G., Cucu, R. G., Dobre, G. M., Podoleanu, A. Gh., Pedro, J., and Saunders, D., 2005, *En-face* optical coherence tomography—a novel application of non-invasive imaging to art conservation, *Optics Express*, **13**, 6133–44.

Liang, H.-D., Cucu, R., Dobre, G. M., Jackson, D. A., Pedro, J., Pannell, Ch., Saunders, D., and Podoleanu, A. Gh., 2004, Application of OCT to examination of easel paintings, *Proceedings of SPIE*, **5502**, 378–81.

Lu, Y., 1996, Lao Xue An Bi Ji, In *Song Ming Ching Shiau Pin Wen Ji Ji Ju*, **1**, 161, Shanghai Yuan Dong Chu Banshe, Shanghai.

Mazurin, O. V., and Porai-Koshits, E. A., 1984, The structure of phase-separated glasses, in *Phase separation in glass* (eds. O. V. Mazurin and E. A. Porai-Koshits), 164–200, Elsevier Science Publishers B. V., North-Holland, Amsterdam.

McCracken, W. J., 1992, Corrosion of glass-ceramics, in *Corrosion of glass, ceramics and ceramic super-conductors* (eds. D. E. Clark and B. K. Zoitos), 432–54, Noyes Publications, Park Ridge.

Shaw, K., 1971, *Ceramic glazes*, Elsevier Publishing, Amsterdam.

Shaw, R. R., and Uhlmann, D. R., 1969, Effect of phase separation on the properties of simple glasses: I. density and molar volume, *Journal of Non-Crystalline Solids*, **1**, 474–98.

Simmons, J. H., 1977, Refractive index and density changes in a phase-separated borosilicate glass, *Journal of Non-Crystalline Solids*, **24**, 77–88.

Targowski, P., 2008, Optical coherence tomography for examination of objects of art, available at website http://www.oct4art.eu.

Targowski, P., Rouba, B., Wojtkowski, M., and Kowalczyk, A., 2004, The application of optical coherence tomography to non-destructive examination of museum objects, *Studies in Conservation*, **49**, 107–14.

Targowski, P., Rouba, B., Gora, M., Tyminska-Widmer, L., Marczak, J., and Kowalczyk, A., 2008, Optical coherence tomography in art diagnostics and restoration, *Applied Physics A*, **92**, 1–9.

Tite, M. S., Freestone, I. C., and Bimson, M., 1984, A technological study of Chinese porcelain of the Yuan dynasty, *Archaeometry*, **26**, 139–54.

Uhlmann, D. R., and Kolbeck, A. G., 1976, Phase separation and the revolution in concepts of glass structure, *Physics and Chemistry of Glasses*, **17**, 146–58.

Vandiver, P. B., 1992, Corrosion and conservation of ancient glass and ceramics, in *Corrosion of glass, ceramics and ceramic super-conductors* (eds. D. E. Clark and B. K. Zoitos), 393–430, Noyes Publications, Park Ridge.

Vandiver, P. B., and Kingery, W. D., 1984, Composition and structure of Chinese Song dynasty celadon glazes from Longquan, *The American Ceramic Society Bulletin*, **63**, 612–16.

Vandiver, P. B., and Kingery, W. D., 1985, Variations in the microstructure and microcompostion of pre-Song, Song, and Yuan dynasty ceramics, in *Ancient technology to modern science, ceramics and civilization*, vol. I (ed. W. D. Kingery), 181–227, The American Ceramic Society, Columbus, OH.

Wiesauer, K., Pircher, M., Gotzinger, E., Hitzenberger, C. K., Oster, R., and Stifter, D., 2007, Investigation of glass-fibre reinforced polymers by polarisation-sensitive, ultra-high resolution optical coherence tomography: internal structures, defects and stress, *Composites Science and Technology*, **67**, 3051–8.

Wood, N., 1999, *Chinese glazes: their origins, chemistry and recreation*, A & C Black/University of Pennsylvania Press, London/Philadelphia.

Yang, M.-L., Lu, C.-W., Hsu, I.-J., and Yang, C. C., 2004, The use of optical coherence tomography for monitoring the subsurface morphologies of archaic jades, *Archaeometry*, **46**, 171–82.

Zhang, Z.-G., Guo, Y.-Y., Zhou, X.-L., and Ruan, M.-L., 2002, Microstructure characteristics of Ru-Guan ware, in *The 2002 International Symposium on Ancient Ceramics* (eds. J.-K. Guo, S.-P. Chen, H.-R. Tan and Y.-Y. Guo), 206–10, Shanghai Research Society of Science and Technology of Ancient Ceramics, Shanghai.